Reversible random sequential adsorption of dimers on a triangular lattice

R. S. Ghaskadvi and Michael Dennin
Department of Physics and Astronomy, University of California at Irvine, Irvine, California 92697-4575
(Received 2 August 1999; revised manuscript received 7 October 1999)

We report on simulations of reversible random sequential adsorption of dimers on three different lattices: a one-dimensional lattice, a two-dimensional triangular lattice, and a two-dimensional triangular lattice with the nearest neighbors excluded. In addition to the adsorption of particles at a rate K^+, we allow particles to leave the surface at a rate K^-. The results from the one-dimensional lattice model agree with previous results for the continuous parking lot model. In particular, the long-time behavior is dominated by collective events involving two particles. We were able to directly confirm the importance of two-particle events in the simple two-dimensional triangular lattice. For the two-dimensional triangular lattice with the nearest neighbors excluded, the observed dynamics are consistent with this picture. The two-dimensional simulations were motivated by measurements of Ca^{2+} binding to Langmuir monolayers. The two cases were chosen to model the effects of changing pH in the experimental system.

PACS number(s): 68.45.Da, 61.43.−j, 64.70.Pf

I. INTRODUCTION

A large number of nonequilibrium systems can be qualitatively described as a flux of particles impinging on a surface or line. Two heavily studied models of such systems treat the particles as either fixed in place upon impact (random sequential adsorption) or as free to diffuse along the surface or line (random cooperative adsorption) [1]. One can also consider the deposition of particles that are free to desorb [2–5]. Some examples of the wide range of applicability of these models include coating problems, chemisorption, physisorption, the reaction of molecular species on surfaces and at interfaces, and the binding of ligands on polymer chains. Jamming is one of the common occurrences in these systems that random sequential adsorption models effectively describe. Loosely speaking, a jammed system is one that is locked into a state of partial coverage because of adsorbate size or shape. In addition to the various adsorption processes, jamming occurs in a wide range of nonequilibrium situations, including glasses, granular materials, and traffic flow [6–8]. In spite of significant progress, no general framework exists for the description of jamming phenomena.

A particular realization of random sequential adsorption is the parking lot model [1,9–12]. In the irreversible version of this model, identical particles (cars) adsorb on a line (curb) at a rate K^+. In this model, the phenomenon of jamming has been known for some time [9]. A certain number of the parked cars leave a space that is too small to fit another car. These are referred to as bad parkers. The result is a density of cars along the curb that is less than 1. The density of cars reached in the irreversible model is the jamming limit.

In the reversible version, identical particles (cars) adsorb on a line (curb) at a rate K^+ and leave the line (curb) at a rate K^-. The removal of cars allows for adjustments in the bad parkers that relieve the jamming. Recently, there has been renewed interest in the reversible case because of its successful application to compaction in granular materials when generalized to three dimensions [13]. In this version, the ''parking spots'' are voids in the material that can be filled with particles. The dynamics of the reversible parking lot model for large values of $K=K^+/K^-$ has a number of interesting features. Perhaps the most dramatic feature is the existence of two very different time scales for the evolution of the coverage fraction of particles [14]. First, there is a rapid approach to a coverage fraction that is equal to the jamming limit. This is followed by a slow relaxation to a larger steady state value. The slow relaxation is understood in terms of collective parking or leaving events involving multiple cars [14].

In this paper, we present the results for simulations of the reversible adsorption of dimers on (1) a one-dimensional lattice, (2) a two-dimensional triangular lattice, and (3) a two-dimensional triangular lattice with the nearest neighbors excluded. The one-dimensional lattice model [12,15–17] was chosen as a test case, and the results are in good agreement with existing data. In particular, our simulations confirm the importance of collective parking events in controlling slow dynamics, as seen in Ref. [14]. The two triangular lattice models exhibit differences in their time evolution that can be attributed to effects of bond orientation and packing on the collective events. The case without nearest-neighbor exclusion corresponds to attempting to cover the plane with a shape formed by two regular hexagons sharing a side. The nearest-neighbor excluded case corresponds to a tiling of distorted hexagons that cover multiple sites.

The rest of the paper is organized as follows. Section II describes the details of the simulations. Section III presents the results for the one-dimensional model. Section IV presents the results for the two triangular lattices. The simulations were motivated in part by experimental measurements of the viscosity of Langmuir monolayers. A brief description of the experimental system and its relationship to the simulations presented here is given in Sec. V. The results are discussed and summarized in Sec. VI.

II. SIMULATION DETAILS

For the one-dimensional simulations, a line of 32 000 particles was used. Both of the triangular lattices consisted of a grid of 1000×1000 particles. To distinguish between the two-dimensional models, we introduce the following nomenclature. Model A will refer to the triangular lattice without

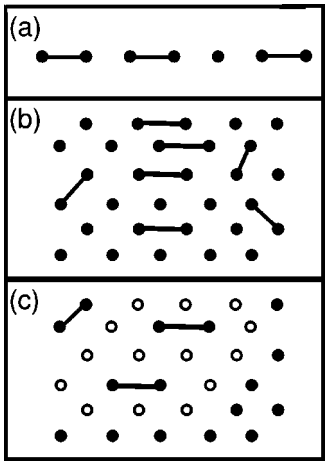

FIG. 1. (a) Example of bonds in the one-dimensional lattice model. The sites are represented by the dots, and the incoming particles are represented by solid lines. The particles form a bond between two neighboring sites. (b) Example of bonds in model A. In this case, particles can bind any two nearest-neighbor sites that are not already part of a bond. (c) Example of bonds in model B. In this case, nearest neighbors of a bound site are not allowed to form bonds. Examples of such sites are represented by open circles.

nearest-neighbor exclusion. Model B will refer to the triangular lattice with nearest-neighbors excluded from binding. Particles are taken to bind to two neighboring sites on the lattice, forming a dimer. The binding occurs at a rate K^+, and particles leave the surface at a rate of K^-.

At each step in the simulation, a site was chosen at random. Then, a random number between 0 and 1 was compared with the ratio $K^+/(K^+ + K^-)$ to determine whether a binding or unbinding event was attempted. For unbinding events, if the chosen site was part of a bond, the bond was broken; otherwise, no action took place. For binding events, a nearest neighbor was randomly selected. A binding event occurred only if both sites were allowed binding sites. The definition of allowed binding site depends on the model. For the one-dimensional and model A cases, an allowed site is any site that is not part of a bond. For model B, if either site is part of a bond or the nearest neighbor of a bound site, binding is not allowed. It is important to note that the number of new bonds created is directly proportional to the number of allowed sites, which is not the same as the number of open sites. The number of desorption events is still directly proportional to the coverage fraction. The coverage fraction, ρ, is defined as the ratio of sites that are part of a bond to the total number of sites.

A schematic of each of the model systems with examples of bound sites is shown in Fig. 1. It is important to notice the different spatial structures in model A and model B. In model A, complete coverage corresponds to all sites being part of a bond. In model B, perfect coverage of the system corresponds to a tile of distorted hexagons that are composed of both empty and bound sites. This results in a maximal coverage fraction $\rho_{max}=0.4$. For both the one-dimensional case and model A, $\rho_{max}=1.0$. In this paper, $\rho(\infty)$ will designate the steady state value of the fractional coverage, and ρ_{jam} will refer to $\rho(\infty)$ in the case $K^-=0$, i.e., the jamming limit.

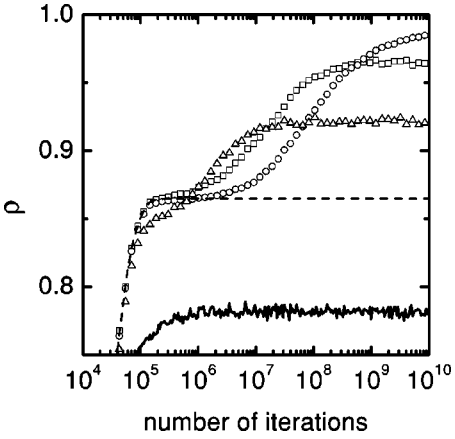

FIG. 2. Shown here is the coverage fraction ρ as a function of the number of iterations for the one-dimensional model. The dashed line represents the evolution for $K^-=0$. The other curves are for solid line ($K=5$), open triangles ($K=40$), open squares ($K=200$), and open circles ($K=1000$).

III. ONE-DIMENSIONAL SIMULATION

Figure 2 shows ρ as a function of the iteration step for selected values of $K=K^+/K^-$. We include the case $K^-=0$, which gives $\rho_{jam}=0.864\,74$. For comparison, analytic calculations give $\rho_{jam}=0.864\,66$ [15,17]. The original work on the reversible parking lot model [12] proposed a mean-field description of the dynamics that can be expressed in terms of the average density, or fractional surface coverage, ρ. Both the continuous and lattice versions of the parking lot model were considered. Figure 3 shows the steady state value of ρ for the values of K plotted in Fig. 2. The solid curve in Fig. 3 is the value for $\rho(\infty)$ for dimers binding to a one-dimensional lattice, as determined by the following equation from Ref. [12]:

$$\rho(\infty)=1-(K^-/K^+)^{1/2}/2. \tag{1}$$

The agreement between our simulations and Eq. (1) confirms the mean-field prediction for the equilibrium values of ρ. However, as with the continuous parking lot model [14], the mean-field description is unable to accurately predict the time evolution of ρ. This can be seen in Fig. 2 where the two time scales controlling the evolution of ρ are evident for K

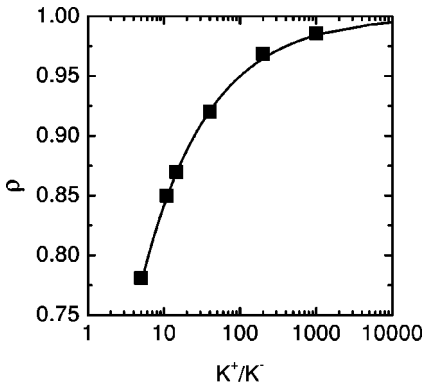

FIG. 3. The solid line is the mean-field prediction for $\rho(\infty)$ as a function of K. The symbols are the values of $\rho(\infty)$ taken from Fig. 2.

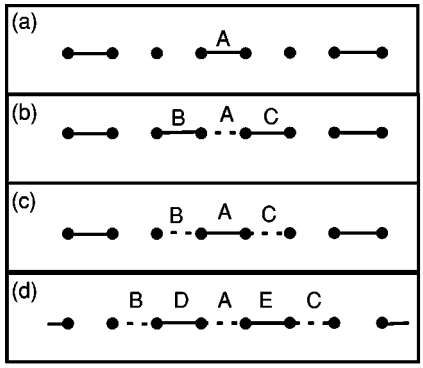

FIG. 4. (a) This illustrates the concept of a ''bad'' parker. The bond at location *A* is the bad parker, as it leaves two sites free. (b) This illustrates a transition from one bad parker to two good parkers. The dashed line represents the original bad parker at location *A* that desorbs. Then, the two good parkers, *B* and *C*, adsorb. (c) This illustrates the two good parkers to one bad parker transition. In this case, the two parkers at *B* and *C* leave and one attaches at *A*. (d) This illustrates a spatial arrangement that corresponds to a two-to-three particle transition. The two possible bond distributions are given by the dashed lines at sites *A*, *B*, and *C* (the good parkers) and the solid lines at sites *D* and *E*, respectively.

>10. The system rapidly reaches ρ_{jam}, and then slowly approaches its equilibrium value. As K goes to infinity, $\rho(\infty)$ approaches 1, but the time to reach equilibrium approaches infinity. This is in agreement with results for the continuous parking lot model reported in Ref. [14].

We have found that the explanation of the two distinct time scales reported in Ref. [14] applies to the discrete case as well. Essentially, collective events are responsible for the evolution of ρ for $\rho>\rho_{jam}$. In Ref. [14], the authors calculated the transition rates for two good particles to one bad particle and one bad particle to two good particles and found that these rates account for the additional slow time scales. In contrast, we directly monitor the transitions as part of the simulation. The reason such transitions result in an additional slow time scale can be understood in terms of the following argument.

As discussed in the introduction, when $K^-=0$, jamming occurs because of ''bad parkers'' that leave empty space. For the one-dimensional lattice, ''empty space'' refers to a single site that is unable to bond. An example is shown in Fig. 4(a). For small values of K^-, bad parkers initially occur at essentially the same rate as for $K^-=0$ because very few particles desorb. Therefore, the coverage fraction for the system quickly approaches a value of ρ_{jam}. Even when a value of ρ_{jam} is reached, the rare desorption event is generally followed immediately by a readsorption because K^+ is so large. The total number of particles is not changed by these events. However, when one bad parker desorbs and two particles adsorb in the opened good locations, then the number of particles is increased by one. Likewise, if two good parkers unbind and one bad parker binds, the number of particles is decreased by 1. Because these events involve multiple particle transitions, they occur on a longer time scale then simple adsorption/desorption events.

For the one-dimensional discrete case, one can identify the relevant good to bad and bad to good transition that involve only two good parkers. These are illustrated in Figs. 4(b) and 4(c). As these events are expected to dominate the dynamics, one can write the following equation for the evolution of ρ once the jamming limit has been reached:

$$d\rho/dt=R_{bg}-R_{gb}+\cdots, \tag{2}$$

[where the ellipsis represents higher-order terms (h.o.t.)]. Here R_{bg} and R_{gb} are the rates of bad to good and good to bad transitions respectively, and $h.o.t$ are collective transitions for a larger number of particles, and hence, occur at a slower rate.

We were able to track the bad to good and good to bad transitions during the simulation. This was accomplished by converting the particle sites to an array of bond locations. Each location between two sites was assigned a value of 1 if a bond was present and 0 if there was no bond. For example, the solid lines in Fig. 4(b) would be represented by the string 1010101. Notice, by definition, between any two bonds there is an open space, so the completely filled system is represented by 1010101010 . . . . The string of bond locations was saved at step i and $i+\Delta$. Each bond location was taken as the initial digit in a seven digit string, and these strings were compared for steps i and $i+\Delta$. We counted the following transitions:

$$1010101\Leftrightarrow 1001001.$$

These transitions correspond to two good to one bad and one bad to two good, as discussed in Figs. 4(c) and 4(b), respectively. The choice of Δ is important. If Δ is too small, the transitions do not have enough time to complete. For example, in the extreme limit of choosing Δ to be a single time step, it is not possible to have multiparticle events, but the total number of bound sites can change by 1. Essentially, Δ must be large enough for the multiparticle transitions to have time to complete. For Δ large enough, the recorded number of transitions is essentially independent of Δ. For the data reported here, we used $\Delta=2\times10^6$.

In addition to counting multiparticle transitions, we also recorded the total change in ρ. Figure 5 compares the actual value of ρ as a function of the number of iterations with the value obtained using Eq. (2) and the computed number of bad to good and good to bad transitions. Once the jamming limit is reached, the bad to good and good to bad transitions account for 94.3% of the change in ρ, confirming the general idea behind Eq. (2). An additional 3.2% of the change in ρ is accounted for by considering a single class of three particle transitions where three good parkers were replaced by two parkers, and the reverse process. These were counted by considering nine digit strings and looking for the transition:

$$101010101\Leftrightarrow 100101001.$$

This curve is also plotted in Fig. 5. The spatial arrangement corresponding to this transition is shown in Fig. 4(d). It is important to note that when bonds exist at sites *D* and *E*, the only way to increase the number of bound sites in this region is for two particles to desorb and three particles adsorb at sites *A*, *B*, and *C*.

IV. TWO-DIMENSIONAL SIMULATIONS

The results of the simulation for ρ as a function of iteration step for the adsorption of dimers on a two-dimensional

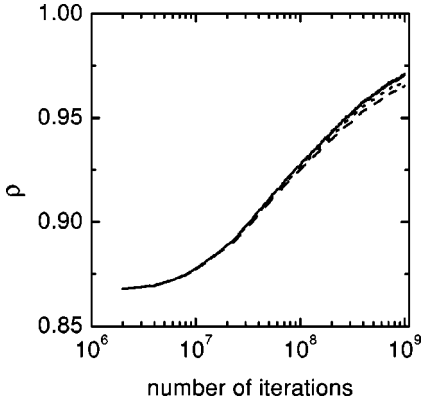

FIG. 5. Shown here is the coverage fraction ρ as a function of the number of iterations for the one-dimensional model and $K=1000$ (solid curve). The curve is plotted starting at the end of the jamming limit plateau. Also plotted are two curves that are obtained by numerically integrating Eq. (2) using the coverage fraction at the jamming limit as the initial state. The dashed line is the result when only the rates for the good to bad and bad to good transitions are included in Eq. (2). These transitions are described in Fig. 4. The dotted line shows the improvement at late times by including a single higher-order transition involving three good parkers converting to two parkers.

triangular lattice (model A) and on a two-dimensional triangular lattice with nearest-neighbor exclusion (model B) are presented in Figs. 6 and 7, respectively. For model A, previous simulations have found a jamming limit of 0.9243 [18]. Our simulations give a value of 0.9120. For model B, we find a jamming limit of 0.275. Recall that complete coverage in this case corresponds to $\rho=0.4$. We are not aware of any previous work on a model B type simulation. However, by appropriately including the empty nearest-neighbor sites in the definition of ρ, we can compare to simulations involving n-mers of length 6 that cover a hexagonal patch. These simulations find a jamming limit of 0.6847, and our converted value is 0.6875 [18].

The results for the two-dimensional cases are qualitatively similar to the one-dimensional case. One observes multiple

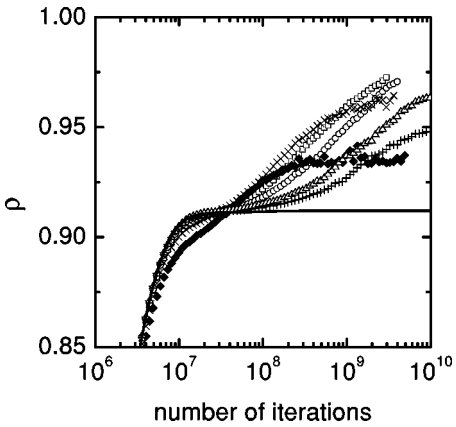

FIG. 6. Shown here is the coverage fraction ρ as a function of the number of iterations for model A. The solid line represents the evolution for $K^-=0$. The other curves are for solid diamonds ($K=200$), crosses ($K=500$), open squares ($K=1000$), open circles ($K=2000$), open triangles ($K=5000$), and plus signs ($K=10\,000$).

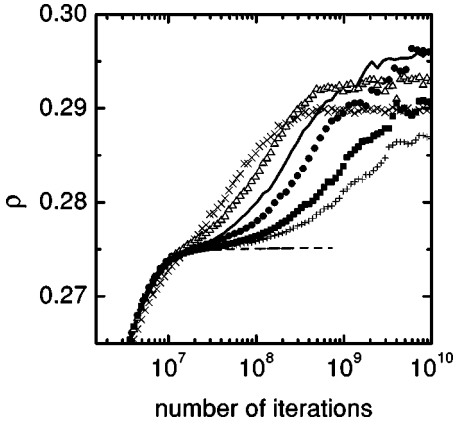

FIG. 7. Shown here is the coverage fraction ρ as a function of the number of iterations for model B. The dashed line represents the evolution for $K^-=0$. The other curves are for crosses ($K=200$), open triangles ($K=500$), solid line ($K=1000$), closed circles ($K=2000$), closed squares ($K=5000$), and plus signs ($K=10\,000$).

time scales: a rapid approach to the jamming limit and a slow relaxation to the steady-state value. This suggests that the same picture of multiparticle transitions will apply to the two-dimensional system. However, in contrast to the one-dimensional case, the identification of collective transitions is significantly more complex for models A and B because of the number of arrangements due to differing orientations of the bonds that can produce bad parkers. However, we did carry out a limited analysis for the case of model A.

The method used to track multiparticle events in model A was similar in concept to the one-dimensional case. However, because the bonds have orientation, we compared the actual sites instead of the bonds for three classes of transitions:

$$0\ 1\ 1\ 0 \Leftrightarrow 1\ 1\ 1\ 1$$

$$\begin{matrix} 0\ 1 & & 1\ 1 \\ 1\ 0 & \Leftrightarrow & 1\ 1 \end{matrix}$$

$$\begin{matrix} 1\ 0 & & 1\ 1 \\ 0\ 1 & \Leftrightarrow & 1\ 1 \end{matrix}$$

In this case, occupied sites are represented by 1 and unoccupied sites are represented by 0. Using sites instead of bonds results in some differences between the methods used in the two-dimensional and one-dimensional cases. First, the transitions counted in this manner correspond to classes of transitions in the following sense. Because we track sites and not bonds, two neareset-neighbor sites can be occupied either because they share a bond or because of two neighboring bonds that are at an angle to the line being considered. So, the first class of transitions includes the transitions that are exactly analogous to the one-dimensional good to bad transitions. But it also includes multiparticle transitions that involve bonds at an angle to the horizontal and that successfully fill the empty sites along the horizontal. Second, the offset of the 1's and 0's in the second two classes of transitions are important and reflect the underlying hexagonal lattice. Note that because only nearest-neighbor bonding is allowed, the diagonal connecting the two zeros in each case is not an allowed binding site. Finally, for the two-dimensional

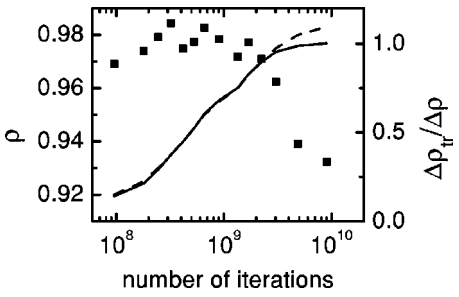

FIG. 8. In this figure, the curves are the coverage fraction ρ versus number of iterations for model A. A reduced grid of 600 by 600 was used to facilitate the counting of collective events. The dashed line is the result of the simulation for $K=5000$. The solid line is the result obtained by tracking two-particle events and integrating Eq. (2) starting at the jamming limit. The symbols are plotted against the right-hand axis and give the ratio of the change in ρ as computed by the two methods. The agreement between the two methods is excellent until approximately 2×10^9 steps. At this point, the contribution to the dynamics of two-particle events decreases dramatically.

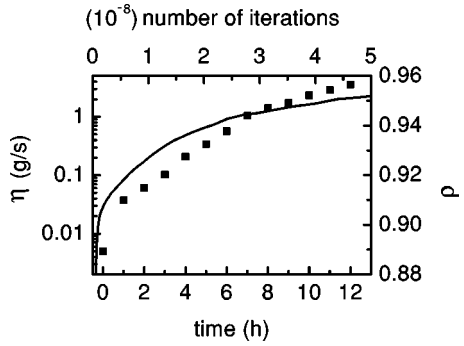

FIG. 9. In this figure, the solid points are taken from Fig. 2 in Ref. [24]. They are the viscosity values (left-hand axis) versus time (bottom axis) for pH=5.5 and a Ca^{2+} concentration in the subphase of 0.65 mM. The solid curve is the simulation data for model A and $K=500$. Plotted here is coverage fraction ρ (right-hand axis) versus number of iterations (top axis).

case, we exploited the hexagonal symmetry of the problem, and multiplied the rate for the first type of transition by 3. The rates of the second two transitions are multiplied by 3/2 to account for double counting. The value of Δ was chosen in a similar fashion to the one-dimensional case and corresponded to a constant interval in $\Delta\rho=0.005$.

The results for ρ as a function of the number of iterations and the value of ρ computed from Eq. (2) using just these three classes of events defined above are plotted in Fig. 8. One striking feature of Fig. 8 is the fact that the two-particle events we identified account for nearly 100% of the dynamics until the number of steps reaches approximately 2×10^9. At this point, the coverage continues to grow, only there is essentially no change due to the identified two-particle events. This strongly suggests other two-particle events or higher-order events involving more than two particles are becoming important.

V. POSSIBLE APPLICATION TO LANGMUIR MONOLAYERS

An obvious question is do the triangular lattices considered here apply to any experimental systems? There is indirect evidence that the models discussed here are relevant to the binding of Ca^{2+} ions to a Langmuir monolayer. Langmuir monolayers are composed of insoluble, amphiphilic molecules that are confined to the air-water interface [19]. They exhibit the usual gas, liquid, and solid phases, as well as a large number of two-dimensional analogs of smectic phases [20]. Many of these phases are hexatic, with the molecules locally arranged on a distorted hexagonal lattice. When Ca^{2+} is present in the water, it can bind two fatty-acid molecules together. This substantially alters a number of the physical properties of the monolayer, such as the lattice spacing and the viscosity [21]. Existing measurements [22] and models [23] of Ca^{2+} binding have focused on the equilibrium coverage fraction. However, the measurements have focused on time scales of 1 h or less. The coverage fraction depends strongly on pH, which is understandable in terms of the degree of ionization of the fatty-acid headgroup. At low values of the pH, essentially all of the fatty-acid molecules are neutral, and the Ca^{2+} ions do not bind. As the pH is increased, an increasing number of fatty-acid molecules become charged, and the Ca^{2+} ions are free to bind to the monolayer.

The possible relevance of models A and B to the fatty-acid monolayers is based on viscosity measurements as a function of time in the presence of Ca^{2+} for the hexatic phase of a particular fatty acid [24]. Figure 9 reproduces one set of data from Fig. 2 of Ref. [24], illustrating a typical time evolution of the viscosity. The viscosity increases 3 orders of magnitude over 15 h. The time evolution can be divided into three distinct regions: an initial rapid rise in viscosity within the first hour, a slower rise in viscosity covering 5 to 6 h, and a final even slower rise in viscosity. For comparison, the computed fractional coverage of ρ is shown in Fig. 9 versus the number of iterations. In this case, we have used a linear scale for the number of iterations. The previous plots all used a logarithmic scale. The time evolution of the Ca^{2+} binding exhibits the three general regions present in the viscosity data, and as such, provides a natural explanation for the effect.

There are a number of points with regard to the connections between the model and the monolayer experiments. The simulations are consistent with the fact that previous measurements of Ca^{2+} binding do not observe multiple time scales. In the simulations, the interesting change in coverage fraction occurs at late times, while in the experiments, only relatively early times are considered [22]. Also, the fact that the experiments agree reasonably well with equilibrium calculations [23] is not surprising because the late-time changes in ρ are relatively small in the simulations. Therefore, longer experiments with more precise measurements of ρ are required to directly observe the effects predicted by our simulations. This discussion naturally leads to the second point: how do small changes in coverage fraction produce large changes in viscosity? An *ad hoc* model that is capable of explaining the large viscosity rise assumes that the viscosity is proportional to $1/(A-\rho)$, where A is a constant determined by the equilibrium coverage fraction. This model is based on the idea that the fluidity (the inverse of the viscos-

ity) is proportional to the number of unbound sites. Clearly, both more careful direct measurements of the coverage fraction versus time and a better theoretical understanding of the connection between viscosity and coverage fraction are needed.

The final two comments concern possible refinements of the adsorption model when applying it to the monolayer system. In this paper, we considered the two cases of binding to any open pair of sites (model A) and binding with nearest-neighbor exclusions (model B) because they are simple cases with different geometric arrangements. The correct detailed description of the Langmuir monolayer system is certainly more complicated than either of these. However, as mentioned, the degree of ionization of the monolayer is pH dependent. To zeroth order, model B is a reasonable description of a monolayer that is only partially ionized for two reasons. First, for a partially ionized monolayer, if a particular site is available for binding, it is highly unlikely that any of the neighbors will be available as well. Second, the steady-state values of ρ found in model B are in reasonable agreement with measurements of the values of ρ reported for monolayers for pH between 5 and 6 [23].

The second refinement concerns lateral diffusion of Ca^{2+} ions once they have bound to the monolayer. Inclusion of diffusion should not substantially alter the qualitative results presented here, but it would effect the quantitative interpretation of the rate constants K^+ and K^-. One can model lateral diffusion of Ca^{2+} as the unbinding of a Ca^{2+} from one of the monolayer molecules followed by a rotation around its remaining bond and subsequent binding to another available site. However, this process could also be viewed as a complete unbinding and rebinding at a neighboring site with a renormalized rate constant. In addition, for ρ to evolve in time, diffusion would need to be coupled with additional binding. This would result in rearrangements that are completely analogous to transitions from one bad parker to two good parkers. Therefore, even with diffusion in the plane of the monolayer, the basic physics remains the same. Jamming will still occur, and the slow relaxation of the bad parkers due to cooperative behavior will result in the slow time scales.

VI. DISCUSSION

Equation (2) provides a means of expanding the dynamics in terms of collective events that occur on slower and slower time scales. We were able to directly confirm this in the simple situation of the one-dimensional model and for the two-particle transitions in model A. For the one-dimensional case, two-particle events were sufficient to describe the dynamics of the system, as was found in the continuous model. This results in two plateaus in the time evolution of the coverage fraction. Single-particle events, dominated by adsorption, rapidly drive the system to the jamming limit. Processes involving two particles are slow enough that ρ plateaus for some time. The length of this plateau is controlled by K, as K ultimately determines the rates of multiparticle transitions. The larger the value of K, the longer the system remains at the jamming limit. After enough time, the two-particle processes have a sufficiently large contribution to the dynamics that ρ increases at a noticeable rate until the true steady-state value is reached, and the coverage plateaus again.

In contrast, one can imagine more complicated dynamics, such as multiple plateaus in the time evolution, occurring when collective events involving three or more particles are important. For example, Fig. 4(d) illustrates the existence of spatial arrangements of unbound sites that cannot be corrected by two-particle events. In model A, Fig. 8 shows that the two-particle events are not capable of bringing the system to its steady-state value, as they are no longer contributing to the dynamics at late enough times. This suggests that the remaining unbound sites occur in spatial arrangements that are analogous to those in Fig. 4(d). Multiple plateaus would arise in the extreme case where the transition rates for two-particle and three-particle events are sufficiently different. This would occur as follows. The two-particle transitions would drive the system to some value ρ_2 in a given time t. If t was small enough compared to the three-particle transition rate, the system would stay at ρ_2 until the three-particle events contributed to the dynamics.

Identifying the existence of multiple plateaus is extremely challenging. First, the steady-state value of ρ must be sufficiently large that at late times the unbound sites are arranged in such a way that two-particle events are ineffective. This implies a sufficiently high value of K. However, this in turn both decreases significantly the rate of collective events and increases the time to reach steady state. For models A and B, we have indirect evidence of multiple plateaus. In both cases, the coverage fraction for $K=10\,000$ appears to be leveling off at a value that is lower than the apparent steady-state values for $K=500$, in the case of model A, and $K=200$, in the case of model B. In principle, $\rho(\infty)$ should approach one (or 0.4 for model B) as K approaches infinity. Therefore, the behavior for $K=10\,000$ suggests the beginning of a secondary plateau. Unfortunately, as discussed, the time required to achieve steady-state increases with K, and we do not have sufficient computing power to determine if this is a true intermediate plateau for $K=10\,000$ or if this is actually the steady-state value.

It is clear that both analytic and more numeric work is needed to fully explore the effects of higher order transitions. Identification of the higher order terms in Eq. (2) is an important step in this process. An exhaustive identification of all possible transitions is beyond the scope of this paper; however, Fig. 10 identifies a small subset of transitions that illustrates why one would expect differences between models A and B for large enough times or large enough values of K.

Figure 10(a) shows a set of transitions for model A, and Fig. 10(b) illustrates the equivalent ones for model B. In both cases, there exists at least two different classes of transitions that turn two good parkers (labeled A, B, and C in Fig. 10) into one bad parker. For model A, if A and C desorb, then there are two possible sites that result in a bad parker, and two possible sites that result in the reestablishment of a pair of good parkers. But, if A and B desorb, then the situation reverts to the one-dimensional case. (In one dimension, after two good parkers desorb, bonding to one out of the three open sites corresponds to the creation of a bad parker [see Fig. 4(c)].) For model B, if A and C desorb, then there are six possible sites that result in a bad parker, and six possible sites that result in the reestablishment of a pair of good parkers. This results in the same probabilities as in model A.

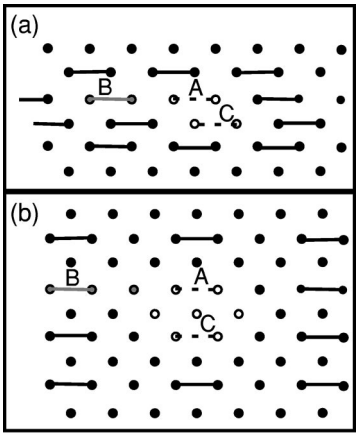

FIG. 10. This figure illustrates collective events in the two-dimensional models. (a) Initially, there are particles at the locations labeled *A*, *B*, and *C*. There are two possibilities. If *A* and *C* desorb, the open circles represent the now available sites. If *A* and *B* desorb, the open circles at *A* and the gray circles are now the available bonding sites. (b) Again, particles are initially at the locations *A*, *B*, and *C*. If *A* and *C* desorb, the open circles represent the now available sites. If *A* and *B* desorb, the open circles at *A* and the gray circles are now the available bonding sites. In this case, there is an additional available site because of the nearest-neighbor exclusion.

However, in the *A* to *B* case, two sites are available for bad parkers, and two sites are available for good parkers. Therefore, the chance of two good switching to one bad is increased. Because differences in transition rates may affect the length of any additional plateaus, detailed calculations of these rates are needed for a fuller understanding of the possible dynamics.

In conclusion, we present results of simulations of the reversible parking lot model for three different lattices. We have directly confirmed the importance of multiparticle transitions for governing the late time behavior in two of the models. The behavior of the third model is consistent with the other two. We discussed the implications of a description of the dynamics in terms of collective events. For the right ratios of transition rates, one would expect to observe multiple plateaus. There is a suggestion of intermediate plateaus in our system, but computational limits prevented any conclusive evidence. One alternative method for finding multiple plateaus would be to consider different particle shapes as a means of adjusting the relative rates of multiparticle transitions. Finally, we presented the possible relevance of the model to the binding of Ca^{2+} to Langmuir monolayers. We showed that the jamming and subsequent slow relaxation of the binding of Ca^{2+} ions is a strong candidate for the source of the long-time scales observed in the viscosity measurements. There are experimental and theoretical details that require further exploration, including direct measurements of the Ca^{2+} coverage fraction, modeling of the dependence of viscosity on Ca^{2+} coverage fraction, better modeling of pH effects, and both measurements and modeling of lateral diffusion. However, given how well the model presented here captures the time scales present in the viscosity data, such future studies should prove extremely fruitful.

ACKNOWLEDGMENTS

We thank Amy Kolan for bringing the parking lot model to our attention, and Chuck Knobler and Robijn Bruinsma for fruitful discussions. This work was supported in part by the NSF through Grant No. CTS-9874701. Acknowledgment by M.D. is made to the donors of The Petroleum Research Fund, administered by the ACS, for partial support of this research.

[1] A large literature has developed in this field. For a review, see J.V. Evans, Rev. Mod. Phys. **65**, 1281 (1993).
[2] For a review, see P. Schaaf, J.C. Voegel, and B. Senger, Ann. Phys. Fr. **23**, 1 (1998).
[3] G. Tarjus, P. Schaaf, and J. Talbot, J. Chem. Phys. **93**, 8352 (1990).
[4] X. Jin, Ph.D. thesis, Purdue University, West Lafayette, IN, 1994.
[5] X. Jin, J. Talbot, and N.H. Linda Wang, AIChE. J. **40**, 1685 (1994).
[6] *Non-Debye Relaxation in Condensed Matter*, edited by T.V. Ramakishnan and M. Raj Lakshmi (World Scientific, Singapore, 1987).
[7] M. Mezard, G. Parizi, and M.A. Virasoro, *Spin Glass Theory and Beyond* (World Scientific, Singapore, 1987).
[8] *Traffic and Granular Flow*, edited by D.E. Wolf, M. Shreckenberg, and A. Bachem (World Scientific, Singapore, 1996).
[9] A. Renyi, Publ. Mat. Inst. Hung. Acad. Sci. **3**, 109 (1958).
[10] X. Jin, G. Tarjus, and J. Talbot, J. Phys. A **27**, L195 (1994).
[11] V. Privman and M. Barma, J. Chem. Phys. **97**, 6714 (1992).
[12] P.L. Krapivsky and E. Ben-Naim, J. Chem. Phys. **100**, 6778 (1994).
[13] E.R. Nowak, J.B. Knight, E. Ben-Naim, H.M. Jaeger, and S.R. Nagel, Phys. Rev. E **57**, 1971 (1998).
[14] A.J. Kolan, E.R. Nowak, and A.V. Tkachenko, Phys. Rev. E **59**, 3094 (1999).
[15] P.J. Flory, J. Am. Chem. Soc. **61**, 1519 (1939).
[16] E.R. Cohen and H. Reiss, J. Chem. Phys. **38**, 680 (1963).
[17] B. Widom, J. Chem. Phys. **44**, 3888 (1966).
[18] Lj. Budinski-Petković and U. Kozmidis-Luburić, Phys. Rev. E **56**, 6904 (1997).
[19] For reviews of Langmuir monolayers, see H. Mohwald, Annu. Rev. Phys. Chem. **41**, 441 (1990); H.M. McConnell, *ibid.* **42**, 171 (1991).
[20] For a review of phase transitions in monolayers, see C.M. Knobler and C. Desai, Annu. Rev. Phys. Chem. **43**, 207 (1992).
[21] M.C. Shih, T.M. Bohanon, J.M. Mikrut, P. Zschack, and P. Dutta, J. Chem. Phys. **96**, 1556 (1992).
[22] K. Kobayashi, K. Takaoka, and S. Ochiai, Thin Solid Films **159**, 267 (1988).
[23] D.J. Ahn and E.I. Franses, J. Chem. Phys. **95**, 8486 (1991).
[24] R.S. Ghaskadvi, S. Carr, and M. Dennin, J. Chem. Phys. **111**, 3675 (1999).